Effect of Earth's Rotation and Range Foldover on Space Based Radar Performance

S. Unnikrishna Pillai, Ph.D., Polytechnic University, Brooklyn, New York
Braham Himed, Ph. D., Air Force Research Laboratory, Rome, New York
Ke Yong Li, C & P Technologies, Inc., Closter, New Jersey

Key Words: space based radar, earth's rotation, crab angle, range foldover, STAP, waveform diversity

ABSTRACT

A space based radar (SBR) by virtue of its motion generates a Doppler frequency component to the clutter return from any point on the earth as a function of the SBR – earth geometry. The effect of earth's rotation around its own axis also adds an additional component to this Doppler frequency. The overall effect of the earth's rotation on the Doppler turns out to be two correction factors in terms of a crab angle affecting the azimuth angle, and a crab magnitude scaling the Doppler magnitude of the clutter patch. Interestingly both factors depend only on the SBR orbit inclination and its latitude and not on the specific location of the clutter patch of interest. Further, it is shown that the crab angle has maximum effect for an SBR on a polar orbit that is above the equator. The crab magnitude on the other hand peaks for an SBR on an equatorial orbit. It is also shown that earth's rotation together with range foldover phenomenon significantly degrade the clutter suppression performance of adaptive processing algorithms. Detailed derivations of these results are presented in this paper.

1. *INTRODUCTION*

Space based radar (SBR) because of its height can cover a very large area on earth for intelligence, surveillance and monitoring of ground moving targets. Once launched into orbit, the SBR moves around the earth while the earth continues to rotate on its own axis. By adjusting the SBR speed and orbit parameters it is thus possible to scan various parts of the earth periodically and collect data. Such an SBR based surveillance system can be remotely controlled and may require very little human intervention. As a result, targets of interest can be identified and tracked in greater detail and/or images can be made with a very high resolution.

In SBR systems, the range foldover phenomenon – clutter returns that correspond to previous/later radar pulses – contributes to the SBR clutter [1, 2, 3, 4]. Another important phenomenon that affects the clutter data is the effect of earth's motion around its own axis [1, 5]. At various points on earth this contributes differently to Doppler, and the modification to Doppler due to earth's rotation is derived in this paper. Detailed performance analysis together with methods to minimize these effects is also presented here.

2. *MODELING EARTH'S ROTATION*

Consider an SBR located at height H above the earth's surface, and for any point of interest D on earth at range R, define the elevation angle θ_{EL} and azimuth angle θ_{AZ} (measured between the SBR velocity vector and the range vector BD) as shown in Fig. 1 and Fig. 2. In this case, the conventional Doppler shift relative to the SBR equals [2, 5]

$$\omega_d = \frac{2V_pT_r}{\lambda/2}\sin\theta_{EL}\cos\theta_{AZ}, \qquad (1)$$

where T_r represents the pulse repetition rate, λ the operating wavelength and $V_p = \sqrt{GM_e/(R_e+H)}$ the SBR speed. Here G is the universal gravitational constant and M_e is the mass of earth.

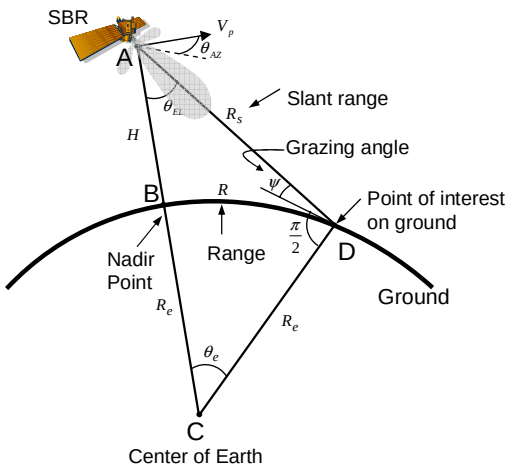

Fig. 1 The parameters of an SBR pointing its mainbeam to a ground point *D*.

As the SBR moves around the earth, the earth itself is rotating around its own axis on a 23.9345 hour basis. This contributes an eastward motion with equatorial velocity of $V_e = \frac{2\pi R_e}{23.9345 \times 3600} = 0.4651$ km/sec.

Report Documentation Page

Form Approved
OMB No. 0704-0188

1. REPORT DATE	2. REPORT TYPE	3. DATES COVERED
01 MAY 2005	**N/A**	**-**

4. TITLE AND SUBTITLE	5a. CONTRACT NUMBER
Effect of Earths Rotation and Range Foldover on Space Based Radar Performance	5b. GRANT NUMBER
	5c. PROGRAM ELEMENT NUMBER
6. AUTHOR(S)	5d. PROJECT NUMBER
	5e. TASK NUMBER
	5f. WORK UNIT NUMBER
7. PERFORMING ORGANIZATION NAME(S) AND ADDRESS(ES) **Polytechnic University, Brooklyn, New York**	8. PERFORMING ORGANIZATION REPORT NUMBER
9. SPONSORING/MONITORING AGENCY NAME(S) AND ADDRESS(ES)	10. SPONSOR/MONITOR'S ACRONYM(S)
	11. SPONSOR/MONITOR'S REPORT NUMBER(S)

12. DISTRIBUTION/AVAILABILITY STATEMENT
Approved for public release, distribution unlimited

13. SUPPLEMENTARY NOTES
See also ADM002017. Proceedings of the 2005 IEEE International Radar Conference Record Held in Arlington, Virginia on May 9-12, 2005. U.S. Government or Federal Purpose Rights License., The original document contains color images.

14. ABSTRACT

15. SUBJECT TERMS

16. SECURITY CLASSIFICATION OF:			17. LIMITATION OF ABSTRACT	18. NUMBER OF PAGES	19a. NAME OF RESPONSIBLE PERSON
a. REPORT	b. ABSTRACT	c. THIS PAGE			
unclassified	**unclassified**	**unclassified**	**UU**	**6**	

Let (α_1, β_1) refer to the latitude and longitude of the SBR nadir point B and (α_2, β_2) those of the point of interest D as shown in Fig. 2 and Fig. 3. As a result, the point of interest D on the earth at latitude α_2 rotates eastward with velocity $V_e \cos\alpha_2$ and this will contribute to the Doppler in (1) as well.

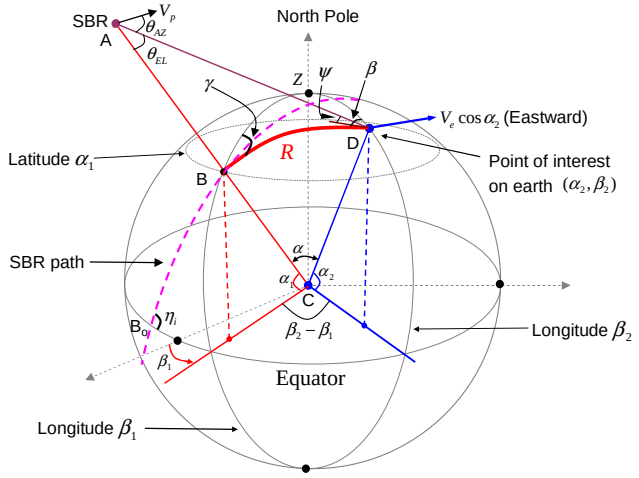

Fig. 2 Doppler contributions from SBR velocity and earth's rotation.

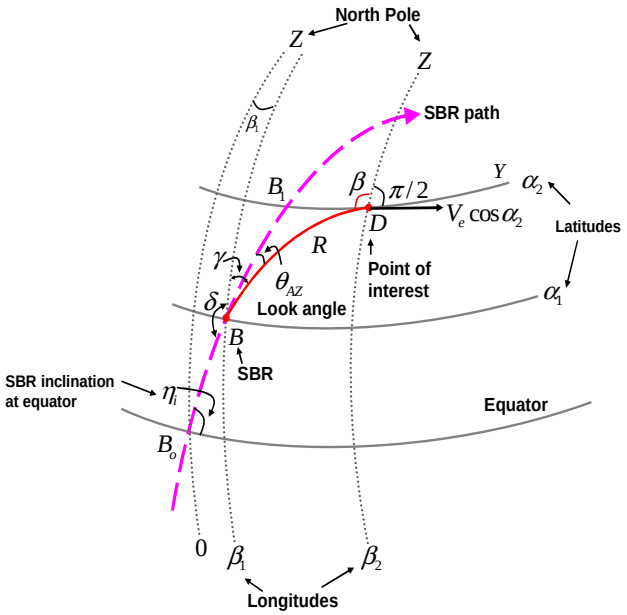

Fig. 3 Effect of earth's rotation on Doppler frequency.

To compute this new component in Doppler shift, note from Fig. 3 that the azimuth angle BDY between the ground range vector R and the earth velocity vector at D equals $(\pi/2+\beta)$ so that $V_e \cos\alpha_2 \cos(\pi/2+\beta) = -V_e \cos\alpha_2 \sin\beta = V_o$ represents the earth's relative velocity at D along the ground range towards B.

Since the grazing angle ψ represents the slant range angle with respect to the ground range at D (see Fig. 2), $V_o \cos\psi = -V_e \cos\alpha_2 \sin\beta \cos\psi$ represents the relative velocity contribution between the SBR and the point of interest D due to the earth's rotation. Together with (1), this gives the modified Doppler frequency that also accounts for the earth's rotation to be

$$\omega_d = \frac{2T_r}{\lambda/2}\left(V_p \sin\theta_{EL} \cos\theta_{AZ} - V_e \cos\alpha_2 \sin\beta \cos\psi\right). \quad (2)$$

To simplify (2), from triangle ACD in Fig. 1 and Fig. 2, we have

$$\frac{\sin(\pi/2+\psi)}{R_e+H} = \frac{\sin\theta_{EL}}{R_e} \text{ and } \cos\psi = \left(1+\frac{H}{R_e}\right)\sin\theta_{EL}, \quad (3)$$

and hence (2) becomes

$$\omega_d = \frac{2V_p T_r}{\lambda/2} \sin\theta_{EL}\left[\cos\theta_{AZ} - \frac{V_e}{V_p}\left(1+\frac{H}{R_e}\right)\cos\alpha_1 \sin\gamma\right], \quad (4)$$

where we have used the identity

$$\cos\alpha_2 \sin\beta = \cos\alpha_1 \sin\gamma \quad (5)$$

that follows from considering the spherical triangle ZBD formed by the intersection of three great circles (see [1] for details). To simplify (4), from Fig. 3 and defining the following triangles $ZBD = \gamma$, $ZBB_o = \delta$ and $B_1BD = \theta_{AZ}$, we have $\gamma = \pi - \delta + \theta_{AZ}$, so that

$$\sin\gamma = \sin\delta \cos\theta_{AZ} - \cos\delta \sin\theta_{AZ} \quad (6)$$

with η_i representing the orbit inclination at the equator for an SBR (see Fig. 3) and considering the spherical triangle ZBB_o, it can be shown that

$$\sin\delta = \frac{\cos\eta_i}{\cos\alpha_1} \text{ and } \cos\delta = -\frac{\sqrt{\cos^2\alpha_1 - \cos^2\eta_i}}{\cos\alpha_1}. \quad (7)$$

Substituting (7) into (4) and simplifying we get the modified Doppler frequency to be [6]

$$\omega_d = \frac{2V_p T_r}{\lambda/2} \rho_c \sin\theta_{EL} \cos(\theta_{AZ} + \phi_c) \quad (8)$$

where

$$\phi_c = \tan^{-1}\left(\frac{\Delta\sqrt{\cos^2\alpha_1 - \cos^2\eta_i}}{1 - \Delta\cos\eta_i}\right), \quad (9)$$

$$\rho_c = \sqrt{1 + \Delta^2\cos^2\alpha_1 - 2\Delta\cos\eta_i}, \quad (10)$$

and

$$\Delta = \frac{V_e}{V_p}(1 + H/R_e). \quad (11)$$

In (8) - (10), ϕ_c represents the crab angle and ρ_c represents the crab magnitude. In summary, the effect of earth's rotation

on the Doppler frequency is to introduce a crab angle and crab magnitude into the SBR azimuth angle and modify it accordingly. Interestingly both these quantities depend only on the SBR orbit inclination and its latitude and *not* on the latitude/longitude of the clutter patch of interest. Eqs. (8) - (10) correspond to the case where the region of interest D is to the east of the SBR path as shown in Fig. 3. If the region of interest is to the west of the SBR path, the crab angle can be shown to be (derivation omitted)

$$\phi_c = -\tan^{-1}\left(\frac{\Delta\sqrt{\cos^2\alpha_1 - \cos^2\eta_i}}{1-\Delta\cos\eta_i}\right), \qquad (12)$$

and the modified Doppler and crab magnitude are as given in (8) and (10), respectively.

The effect of crab angle on Doppler as a function of range for different azimuth angles is shown in Fig. 4.

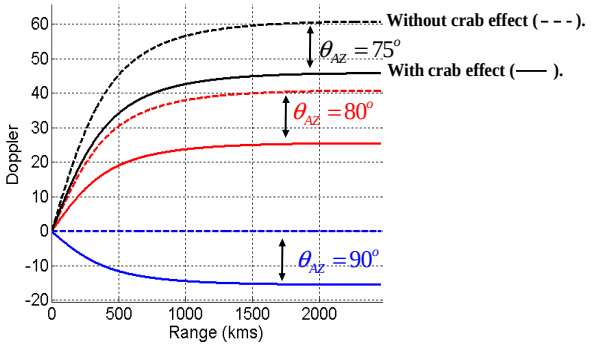

Fig. 4 Effect of crab angle on range-Doppler.

As (8) shows, the effect of earth's rotation is to shift the azimuth angle appearing in the Doppler by approximately $\phi_c = \pm 3.77^o$ and simultaneously modify the Doppler magnitude as well. As a result, even for $\theta_{AZ} = 90^o$, the Doppler peak values occur away from $\omega_d = 0$, depending upon the range. This shift in Doppler with and without crab effect is illustrated in Fig. 4 for various azimuth angles. The actual Doppler frequencies of the incoming clutter will depend upon the Doppler foldover parameter β for the array configuration given by $\beta = 2V_p T_r/(\lambda/2)$ [1, 5, 7].

3. *RANGE FOLDOVER and EARTH'S ROTATION*

When range foldover and earth's rotation are present simultaneously, distinct Doppler frequencies are generated from the associated range foldover points (see Fig. 5). These range foldover points will project different gains depending on their position with respect to the array gain pattern. For every range point of interest, the two phenomena together generate a sequence of Doppler frequencies. For example, at $PRF = 500\,\text{Hz}$, there are seven range foldover Doppler frequencies for an SBR located at a height of 506 km above the earth's surface.

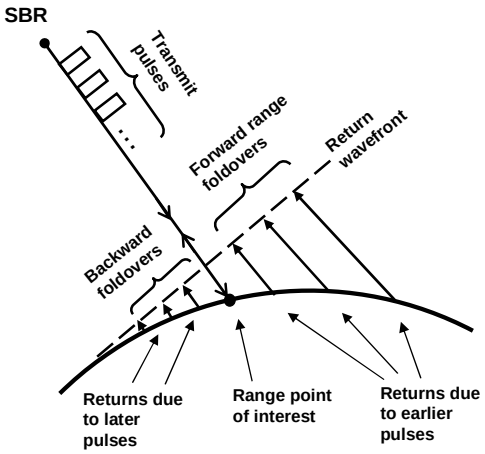

Fig. 5 Range foldover phenomenon.

The clutter corresponding to these range bins will be associated with these modified Doppler frequencies. To illustrate the limitations imposed on processing gains due to earth's rotational phenomenon and range foldover, Fig. 7 and Fig. 8 show the matched filter (MF) output in terms of ideal *SINR* loss *without* and *with* range foldover and earth's rotation. Recall that the *SINR* loss is defined as [3, 5, 7]

$$SINR = \boldsymbol{s}^H(c,\,\omega_d)\,\boldsymbol{R}^{-1}\,\boldsymbol{s}(c,\,\omega_d) \triangleq \boldsymbol{s}^H\,\boldsymbol{R}^{-1}\,\boldsymbol{s}. \qquad (13)$$

(The superscript H denotes the complex conjugate transpose operation). Here $\boldsymbol{s}(c,\,\omega_d)$ represents the normalized space time steering vector for the desired point of interest located at $\boldsymbol{\theta} = (\theta_{EL},\,\theta_{AZ})$ that corresponds to the cone-angle

$$c = \sin\theta_{EL}\cos\theta_{AZ}, \qquad (14)$$

and Doppler frequency ω_d for the SBR configuration under consideration. For a uniformly spaced array consisting of N elements, the space-time steering vector is given by

$$\boldsymbol{s}(c,\,\omega_d) = \boldsymbol{b}(\omega_d)\otimes\boldsymbol{a}(c), \qquad (15)$$

where

$$\boldsymbol{a}(c) = \frac{1}{\sqrt{N}}[1,\ \upsilon,\ \upsilon^2,\ \cdots,\ \upsilon^{N-1}]^T, \qquad (16)$$

$$\upsilon = e^{-j\pi d\sin\theta_{EL}\cos\theta_{AZ}} = e^{-j\pi dc}, \qquad (17)$$

and d represents the inter-element distance normalized to half wavelength. Further, for a data vector containing M pulses

$$\boldsymbol{b}(\omega_d) = \frac{1}{\sqrt{M}}[1,\ \lambda,\ \lambda^2,\ \cdots,\ \lambda^{M-1}]^T \qquad (18)$$

where $\lambda = e^{-j\pi\omega_d}$. The ideal clutter covariance matrix $\boldsymbol{R} = E\{\boldsymbol{x}\,\boldsymbol{x}^H\}$ corresponding to an $MN\times 1$ clutter data vector $\boldsymbol{x}$ at a specific range R_o has the form

$$\boldsymbol{R} = \sum_{k}\sum_{m=0}^{N_a} P_{km} G(\boldsymbol{\theta}_{km}) \boldsymbol{s}_{km}\boldsymbol{s}_{km}^H + \sigma^2 \boldsymbol{I} \qquad (19)$$

where the inner summation is over the N_a range foldovers at R_1, R_2, $\cdots$, and the outer summation is over all azimuth angles $\theta_{AZ,k} = \theta_{AZ} + k\Delta\theta$, $k = \pm 1, \pm 2, \cdots$, of interest. Here, $G(\boldsymbol{\theta}_{km})$ and P_{km} correspond to the array gain and clutter power from the $(k, m)^{th}$ ground patch at $\boldsymbol{\theta}_{km} = \left(\theta_{EL_m}, \theta_{AZ_k}\right)$, respectively. The associated steering vector is given by $\boldsymbol{s}_{km} = \boldsymbol{s}\left(c_{km}, \omega_{d_{km}}\right)$, where the cone angle for the $(k,m)^{th}$ patch equals $c_{km} = \sin\theta_{EL_m}\cos\theta_{AZ_k}$ and the corresponding Doppler frequency is given by (from (1) or (8))

$$\omega_{d_{km}} = \begin{cases} \beta c_{km}, & \text{w/ earth's rotation,} \\ \beta \rho_c \sin\theta_{EL_m}\cos(\theta_{AZ_k} + \phi_c), & \text{w/o earth's rotation,} \end{cases} \qquad (20)$$

depending on whether earth's rotation is absent or present in Eq. (19). Fig. 6 shows Doppler as a function of the cone angle *with* and *without* earth's rotation. Note that in the absence of earth's rotation, there is a one-to-one correspondence between Doppler and cone angle. As a result, points that project the same cone angle in the range-azimuth domain generate identical Doppler. Thus, all points on the iso-cone plot (see Fig. 9 (a)) project the same Doppler frequency. However, in the presence of earth's rotation, this is no longer true, and for a given cone angle, different range foldovers generate different Doppler frequencies. This results in Doppler spread as shown in Fig. 6, which displays the entire band of Doppler curves corresponding to all range points of interest and their foldovers as a function of azimuth angle. It is seen that in the limit, they generate a continuous band of Doppler frequencies. In summary, in the presence of earth's rotation, every point on earth projects a different Doppler that is confined within a band of frequencies.

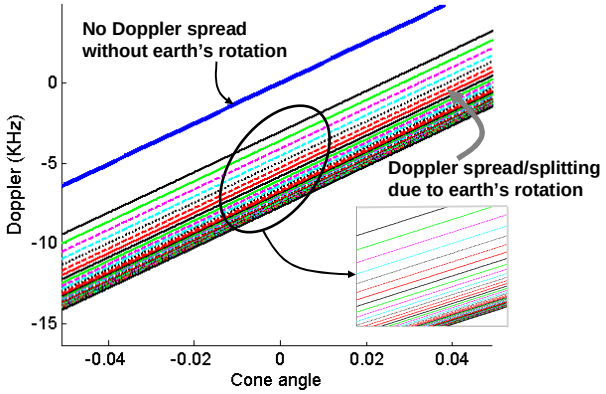

Fig. 6 Doppler spitting due to earth's rotation.

Fig. 7 shows the ideal *SINR* performance as a function of range and Doppler *with* and *without* range foldover and earth's rotation. Note from Fig. 7 (c) that the resulting known bias can be adjusted, if necessary, to reflect the normalized performance as shown in Fig. 7 (a). However, this is not the case in Fig. 7 (d), which shows a severe performance degradation when *both* range foldover and earth's rotation are jointly present.

This effect can also be seen in Fig. 8, which corresponds to a range of 2,400 km. It is seen that performance in terms of clutter nulling is significantly inferior when both these phenomena are simultaneously present. This is evidently the case in practice, which presents a significant challenge for target detection [5, 6].

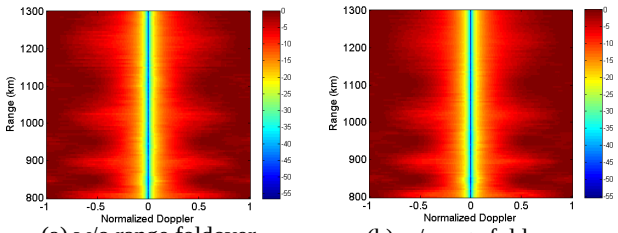

(a) w/o range foldover, w/o earth's rotation

(b) w/ range foldover, w/o earth's rotation

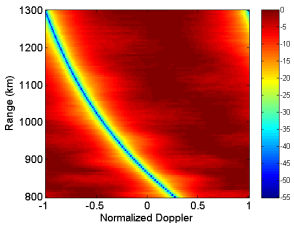

(c) w/o range foldover, w/ earth's rotation

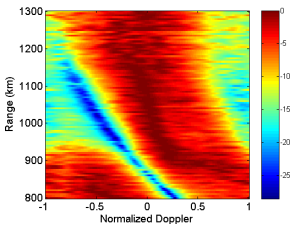

(d) w/ range foldover, w/ earth's rotation

Fig. 7 Matched filter output *with* and *without* range foldover and earth's rotation, SBR height *H* = 506 km, *PRF* = 500 Hz, and $\theta_{AZ} = 90^o$.

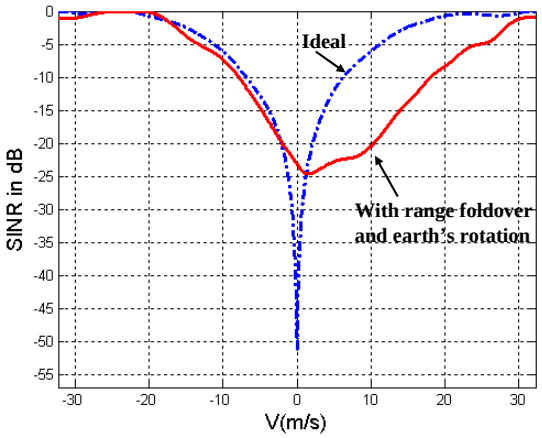

Fig. 8 Matched filter output *with* and *without* (ideal) range foldover and earth's rotation, range = 2400 km and $\theta_{AZ} = 90^o$.

To understand why the clutter notch widens in the presence of earth's rotation as shown in Fig. 8, it is necessary to review (13) - (20) simultaneously. Fig. 8 is plotted for a fixed $\left(R_o, \theta_{AZ_o}\right)$, which fixes the cone angle *c* in (14) while varying ω_d in (18). As a result, the cone angle

$$c_o = \sin\theta_{EL_o}\cos\theta_{AZ_o} \tag{21}$$

remains fixed. However, referring to (19) and (20), there are several other points $\left(R_o, \theta_{AZ_o}\right)$ or equivalently locations at $\left(\theta_{EL_k}, \theta_{AZ_k}\right)$ that satisfy the identity

$$c_o = \sin\theta_{EL_k}\cos\theta_{AZ_k}. \tag{22}$$

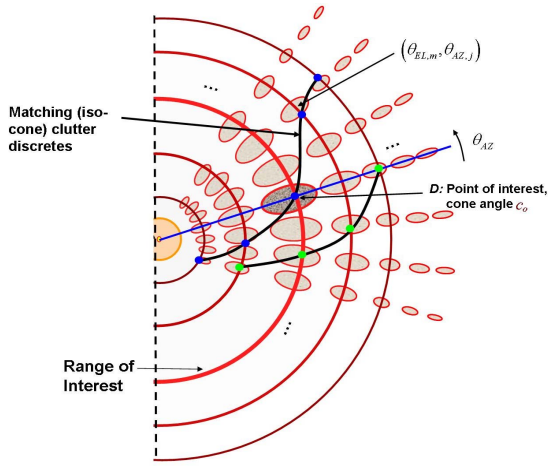

(a) Range foldover and matching clutter discretes

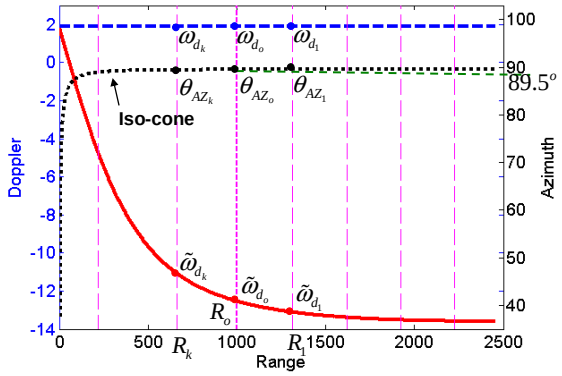

(b) Projected Doppler at $R_t = 1000$ kms, $\theta_{AZ} = 89.5^o$

Fig. 9 Projected Doppler frequencies *with* and *without* earth's rotation.

These iso-cone contours are superimposed on the array gain pattern in Fig. 9 (a), which shows the multiple solutions given by (22). The dotted lines in Fig. 9 (b) show the iso-cone contours given in (22) for $\theta_{AZ_o} = 89.5^o$. These specific points give the best match for the spatial part of the steering vector in (13) - (17), and hence they contribute the maximum towards the null in Fig. 8. However, the Doppler projected by these points satisfy (1) or (8) depending upon whether earth's rotation is *absent* or *present* (see (20)). Thus, in the absence of earth's rotation, the projected Doppler at these selected points ω_{d_k} *agree* with ω_{d_o}, the Doppler associated with $\left(R_o, \theta_{AZ_o}\right)$ exactly (see dashed lines in Fig. 9 (b)). This gives a perfect match together with the temporal part of the steering vector in (13) - (16) resulting in a simple single null in Fig. 8 (ideal case). However, in the presence of earth's rotation, the projected Doppler values $\tilde{\omega}_{d_{km}} = \beta\rho_c \sin\theta_{EL_m}\cos(\theta_{AZ_k} + \phi_c)$ at these selected points are *different* from the Doppler associated with $\left(R_o, \theta_{AZ_o}\right)$ as seen from the solid curves in Fig. 9 (b). Hence, secondary nulls occur at $\tilde{\omega}_{d_1}, \tilde{\omega}_{d_2}, \ldots$, and when taken together they result in a wider clutter null (see Fig. 8).

The problem is thus to rectify the situation in Fig. 7 (d), so that it becomes closer to the symmetric curves of Fig. 7 (a), (b), and (c). Having both range foldover and earth's rotation at the same time results in unacceptable performance degradation as shown in Fig. 7 (d) - Fig. 8; whereas when either one is present separately, the effect can be rectified.

4. *ORTHOGONAL PULSING SCHEME*

We propose to use waveform diversity on the sequence of transmitted radar pulses to realize the above goal by suppressing the range foldover returns. Recall that in ordinary practice, a set of identical pulses are transmitted. To suppress returns due to range foldover, for example, individual pulses $f_1(t)$, $f_2(t)$, $\cdots$, can be made orthogonal to each other so that

$$\int_o^{T_o} f_i(t) f_j(t)\, dt = \delta_{i,j}, \quad i, j = 1, 2, \cdots, N_a, \tag{23}$$

where N_a is the maximum number of distinct range foldovers present in the data and $\delta_{i,j}$ is the Kronecker delta product. Then, with appropriate matched filtering [8], the range ambiguous returns can be minimized from the main return corresponding to the range of interest. In this case, performance will be closer to that shown in Fig. 7 (c). Note that for range foldover elimination, waveform diversity needs to be implemented only over N_a pulses. For an SBR located at a height of 506 km and an operating $PRF = 500$ Hz, $N_a \approx 7$. This is the case since matched filtering will eliminate the superimposed range foldover returns since they correspond to waveforms that are orthogonal to the one in the mainbeam.

Fig. 10 shows the *SINR* improvement using eight up/down chirp waveforms all with equal bandwidth [8].

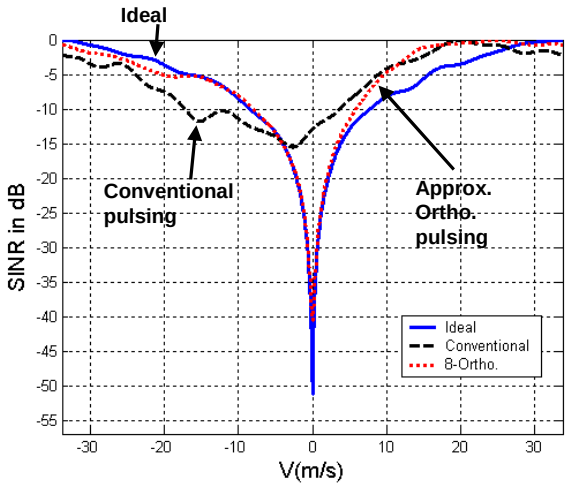

Fig. 10 *SINR* performance improvement, range = 1200 km.

These waveforms are either up/down ramps or triangular in shape in the frequency domain. Quadrature phase shifting of these waveforms will generate an additional set of four waveforms, resulting in a pool of eight waveforms. Notice that these eight waveforms are only approximately orthogonal. However, they all maintain the desirable pulse compression property. In this case, although the performance has improved over the conventional pulsing scheme considerably, the remaining degradation can be attributed to the approximate orthogonal nature of these waveforms.

Fig. 11 (b) shows the improvement in *SINR* as a function of range and Doppler obtained by using these chirp waveforms. For comparison purposes, Fig. 11 (a) shows the performance using conventional pulsing in the presence of both range foldover and earth's rotation. Note that using waveform diversity on transmit, the performance shown in Fig. 11 (b) is restored to that shown in Fig. 7 (c), where only earth's rotation present.

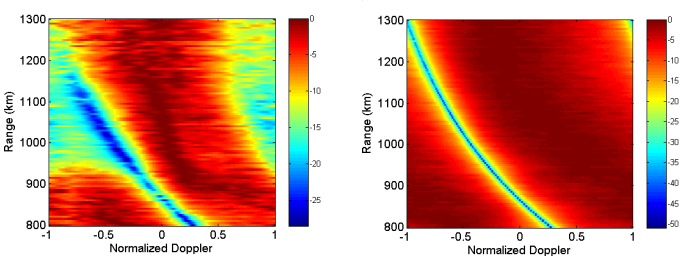

(a) Conventional (b) Eight chirp waveforms

Fig. 11 Matched filter output *SINR* with range foldover and earth's rotation for two different pulsing schemes (a) Conventional pulsing [same as Fig. 7 (d)], (b) Eight chirp waveforms that are approximately orthogonal.

In summary, using waveform diversity on transmit, it is possible to eliminate the effect of range foldover with performance results as shown in Fig. 11 (b). This situation on the other hand corresponds to that shown in Fig. 7(c), where a known crab angle generates the range dependency on the Doppler. As a result, using an appropriate inverse compensation factor, it is possible to correct this Doppler dependency. The resulting performance will be approximately the same as the performance shown in Fig. 7 (a), indicating that using waveform diversity on transmit, it is possible to achieve performance close to the ideal case even in the presence of both range foldover and earth's rotation. The results presented here correspond to the case where the ensemble averaged clutter covariance matrix is given. The case where the covariance matrix is estimated from secondary data is under investigation.

5. *CONCLUSIONS*

This paper gives a detailed derivation for modeling earth's rotation on SBR Doppler. The overall effect of earth's rotation on Doppler can be modeled as two correction factors in terms of a crab angle affecting the azimuth and a crab magnitude affecting the Doppler magnitude of the clutter path. The earth's rotation together with range foldover significantly degrade the clutter suppression performance of adaptive processing algorithms, thus making for target detection more difficult. Waveform diversity on transmit is shown to minimize these effects and restores performance close to that of the ideal case.

ACKNOWLEDGMENTS

Research reported here was partially supported under contracts F30602-03-C-0136 and FA8750-04-C-0202.

REFERENCES

[1]. K. Y. Li *et. al.*, "STAP for Space Based Radar", *Air Force Research Laboratory Final Technical Report*, AFRL-SN-RS-TR-2004-170, June 2004

[2]. M. E. Davis and B. Himed, "L Band Wide Area Surveillance Radar Design Alternatives", *International Radar 2003 – Australia*, September. 2003.

[3]. M. E. Davis, B. Himed, and D. Zasada, "Design of Large Space Radar for Multimode Surveillance", *IEEE Radar Conference*, Huntsville, AL, pp. 1-6, May 2003.

[4]. J. Maher, M. E. Davis, R. J. Hancock, and S. W. Theis, "High Fidelity Modeling of Space-Based Radar", *2003 IEEE Radar Conference*, Huntsville, AL, pp. 185-191, May 2003.

[5]. P. Zulch, M. E. Davis, L. Adzima, R. J. Hancock, and S. W. Theis, "The Earth Rotation Effect on a LEO L-Band GMTI SBR and Mitigation Strategies", *IEEE Radar Conference*, Philadelphia, PA, April 2004.

[6]. S. U. Pillai, B. Himed, K. Y. Li, "Waveform Diversity for Space Based Radar", *Proc. of Waveform Diversity and Design*, Edinburgh, Scotland, Nov 8-10, 2004.

[7]. J. R. Guerci, *Space-Time Adaptive Processing for Radar*, Artech House, Boston, 2003.

[8]. S. U. Pillai, B. Himed, K. Y. Li, "Orthogonal Pulsing Schemes for Improved Target Detection in Space Based Radar", *2005 IEEE Aerospace Conference*, Big Sky, MT, March 5-12, 2005,

BIOGRAPHIES

S. Unnikrishna Pillai is a Professor of Electrical and Computer engineering at Polytechnic University, Brooklyn, New York. His present research activities include radar signal processing, blind identification, spectrum estimation, system identification and space based radar signal processing.

Braham Himed is a senior research engineer with the United States air force research Laboratory, sensors directorate. His research interests include detection, estimation, multichannel adaptive signal processing, time series analyses, array processing, space-time adaptive processing, hot clutter mitigation, and ground penetrating radar technology.

Ke Yong Li is a staff engineer with C & P Technologies, Inc., New Jersey specializing in radar signal processing. His research interest includes Space Time Adaptive Processing (STAP), Optimum Trans-Receiver design technology and space based radar signal processing.